Molecular Insight into Silk Fibroin Based Delivery Vehicle for Amphiphilic Drugs: Synthesis, Characterization and Molecular Dynamics Studies

Mercedes G. Montalbán[a], Sandipan Chakraborty[b], Jorge Peña-García[c], Hugo Verli[d], Gloria Villora Cano[a], Horacio Pérez-Sánchez[c,*], F. Guillermo Díaz-Baños[e,*]

[a] *Department of Chemical Engineering, University of Murcia, Murcia, Spain*

[b] *Department of Physical Chemistry, Indian Association for the Cultivation of Science, Kolkata, India*

[c] *Bioinformatics and High Performance Computing Research Group (BIO-HPC), Computer Engineering Department, Universidad Católica San Antonio de Murcia (UCAM), Murcia, Spain*

[d] *Centro de Biotecnologia, Universidade Federal do Rio Grande do Sul, Avenida Bento Gonçalves 9500, CP 15005, Porto Alegre, 91500-970, RS, Brazil*

[e] *Department of Physical Chemistry, University of Murcia, Murcia, Spain*

*Corresponding authors to whom correspondence should be addressed:

Horacio Pérez-Sánchez: hperez@ucam.edu Tel: +34-9682788819; F. Guillermo Díaz-Baños: fgb@um.es Tel: +34-8687394.

ABSTRACT

Recent emergence of natural biopolymers as drug delivery vehicles is attributed to their biodegradability and less systemic toxicity. Here, we have synthesized curcumin, indomethacin and emodin-loaded silk fibroin nanoparticles (SFNs) and characterized several pharmacokinetic parameters (Drug Loading and Encapsulation Efficiency). Silk fibroin is a highly promising bio-material with impressive mechanical properties, high bio-compatibility and it does not exert any immunological responses *in vivo*. Our results show that emodin almost released completely within 144 hr, however a steady release profile has been observed for indomethacin which is attributed to its moderate loading and encapsulation efficiency by SFNs. On the other hand, complete release of curcumin is not observed even in 168 hr. Curcumin also shows very promising drug loading and encapsulation efficiency when loaded within the SFNs matrix. Molecular level characterization with the aid of blind docking and molecular dynamics simulation reveals that the encapsulation efficiency of the drugs exactly follows the interaction energy patterns obtained from MM/PBSA calculation, i.e., curcumin > indomethacin > emodin. Strong binding energy of curcumin with the fibroin protein is attributed to the formation of more number of hydrogen bonds compared to the other two drugs and involvement in additional π-π stacking interactions. Indomethacin interacts moderately with the SFN primarily mediated through several van der Waals interactions which accounts for its sustained release from the SFN

matrix. Emodin interacts with the fibroin protein very weakly which is responsible for its low encapsulation and observed diffusion controlled release behavior within the fibroin matrix.

Keywords: Encapsulation; Drug Loading, Blind Docking, Molecular Dynamics.

1. Introduction

Drug delivery systems are often used to improve the pharmacokinetic properties, bioavailability and tissue distributions of xenobiotics.[1] Novel approaches or formulations are often used to improve quantity of drugs at the target site as well as increase drug response duration.[2-4] Particularly, amphiphilic drugs are often demonstrate limited efficacy in preclinical and clinical studies mainly due to their low bioavailability, which results in sub-therapeutic concentrations at the target site. Various advanced drug delivery systems, such as nanoparticles,[5, 6] liposomes,[4] microparticles[7, 8] and implants[9-11] have been designed to enhance the therapeutic efficacy of many drugs by increasing their bioavailability and thereby increasing the effective dosage at the target site. Synthetic drug carriers demonstrate high stability and carrier capacity.[5] They are capable of incorporating both hydrophilic and hydrophobic drugs and can be administered through various routes, including oral administration and inhalation. These carriers can also be designed to enable controlled (sustained) drug release from the matrix. However, synthetic polymer based drug carriers are often induce toxicity[12] and non-degradability as well as complicated synthetic process is a problem associated with the synthetic nanocarriers.

Recently, natural biopolymers based delivery vehicles come into the focus due to their biodegradability, low toxicity and also they are environmentally friendly.[3] They are capable of encapsulating wide varieties of molecules. In this context, silk fibroin based materials have

gained tremendous attention in last few years as an attractive biomaterial in biomedical[13-17] and tissue engineering applications[18] due to their excellent biocompatibility and mechanical properties.[19-21] Silk fibroin is obtained from *Bombyx mori* cocoons and can be highly fabricated as braided, knitted and non-woven materials.[20] Silk fibroin materials are highly bio-compatible and do not exert any immunological responses *in vivo*.[16, 19, 21] They promote adhesion, growth and proliferation of different cell types.[16, 19] Naturally produced silk fibroin has impressive mechanical properties with Young's modulus of 10-17 Gpa, large breaking strain and toughness of 70-78 MJ/m^3 which is higher than the synthetic polymers.[20] Moreover, the particle size of the fibroin materials can be easily modulated by mild processing under ambient condition.[22] Silk fibroin based particulate materials have potential applications in medicine for their ability to adsorb, transport, and deliver a wide range of bioactive molecules.[13, 15, 23]

Remarkable mechanical properties and ability to morph in different size and shape which is highly controllable is attributed to its amino acid compositions and 3-D structural arrangements of silk fibroin. The protein is composed of a long H-chain and a short L-chain attached together by disulphide bonds.[20] The H-chain contains 12 hydrophobic repeats separated by 11 hydrophilic regions. Hydrophobic region contains mostly ALA, GLY and SER whereas hydrophilic domains contain amino acids in non-repetitive arrangements.[20] The hydrophobic regions are adopting β-sheet crystallites which are stabilized by intra-molecular as well as intermolecular hydrogen bonding and van der Waals interactions whereas the non-repetitive hydrophilic regions form the semi-amorphous region of silk fibroin. Combination of both semi-amorphous domain and β-sheet crystallites dictates the strength and stiffness of silk-fibroin materials. Silk fibroin solution can be used to regenerate silk material with various morphologies like sponges, hydrogels, mats

and films. However, during the process of reconstruction it often loses mechanical properties to some extent due to the degumming and dissolution processes.

In the present work, we have considered three amphiphilic drugs: curcumin, indomethacin and emodin. Curcumin, a diarylheptanoid, is the principal component of turmeric. It is commonly used as dietary supplements and food additves. Curcumin is a strong anti-oxidant[24] which also demonstrates anti-cancer,[25] anti-inflammatory,[26, 27] neuroprotective[28-30] and many more health beneficial activities.[31] Indomethacin is a FDA approved non-steroidal anti-inflammatory drugs commonly used to reduce pain, fever.[32, 33] Emodin, 1,3,8-Trihydroxy-6-methylanthracene-9,10-dione, is a major component of *Aloe vera*. It demonstrates strong anti-cancer, hepatoprotective and anti-inflammatory activities.[34-36] We have synthesized and characterized curcumin, indomethacin and emodin-loaded silk fibroin nanoparticles (SFNs) by spray technology and characterize several pharmacokinetic parameters (Drug Loading Content and Encapsulation Efficiency) of the encapsulated drugs. Atomistic simulations have been used to elucidate silk-drug interactions to provide mechanistic insight into the process.

2. Materials and methods

2.1. Generation of silk-fibroin

White *Bombyx mori* silk cocoons were reared in the sericulture facilities of the IMIDA (Murcia, Spain) and raised on a diet of natural *Morus alba L.* fresh leaves. In order to obtain silk fibroin, raw silk cocoons were boiled twice in a 0.05M Na_2CO_3 aqueous solution for 45 minutes. The remaining silk fibroin was rinsed thoroughly with ultrapure water and dried prior to use. Silk fibroin was dissolved in the ionic liquid 1-ethyl-3-methylimidazolium acetate using ultrasound as described by Lozano-Pérez et al.[37] The ionic liquid (95% purity) was purchased from IoliTec

GmbH (Germany) and was used without further purification. Curcumin (99% purity) was purchased from ChromaDex (Irvine, CA) and indomethacin (99% purity) and emodin (95% purity) were supplied by Sigma-Aldrich. Purified water (18.2 MΩ·cm at 25ºC; from a Millipore Direct-Q1 ultrapure water system, Billerica, MA) was used throughout the study. All other chemicals and solvents were of analytical grade and were used without further purification.

2.2. Preparation of silk fibroin nanoparticles

Preparation of silk fibroin nanoparticles (SFNs) was based on the method described previously by Zhang et al.[38] with modifications. Briefly, 3 ml of ultrapure water (MilliQ, 18.2 MΩ·cm) was slowly added to the freshly prepared silk-ionic liquid solution to reduce the viscosity. The solution was heated at 60ºC and the silk-ionic liquid solution was then propelled using a peristaltic pump and was sprayed onto 100 mL of gently stirred MeOH at -20ºC by a thermostatically controlled 0.7 mm two-fluid nozzle (from a Mini Spray Dryer B-290, BÜCHI Labortechnik, Switzerland, Part No. 044698) which uses compressed N_2 to disperse the solution into fine droplets. A milky white suspension appeared and the suspension was allowed to reach room temperature while stirring for 2 hours. Then, the particle suspension was transferred to centrifuge vials and centrifuged at 13400 rpm for 15 minutes, at 4ºC (Sigma 3-18K Centrifuge with a 19776 H angle rotor). The supernatant (free of particles) was removed, filtered (0.22- mm disposable PTFE filters) and reserved for subsequent recycling of the ionic liquid. An equal volume of fresh methanol was added to the vial, and the white precipitate was suspended by vigorous stirring in a vortex mixer for 2 minutes followed by 5 min of ultra-sonication with a Branson 450D sonicator. The centrifugation was repeated under the same conditions. The white precipitate was subjected to successive rinses with ultrapure water to remove the rests of

methanol and ionic liquid. The particles were lyophilized in an Edwards Modulyo 4K Freeze Dryer for 72 hours, at -55ºC and 0.5 mbar in order to obtain dry particles. The methanolic fractions were mixed before recovery of the ionic liquid, by removal of the methanol/water on a BÜCHI RE-111 rotary evaporator at 80ºC and 80 mbar. The ionic liquid was kept in a desiccator until reuse.

2.3. Loading of the drug in the silk fibroin nanoparticles

Loading of the drugs (curcumin, indomethacin or emodin) were carried out by physical adsorption. 40 ml of 1 mg/ml solution of curcumin, indomethacin and emodin in ethanol were used to re-suspend 325 mg of silk fibroin nanoparticles. The suspension was then sonicated for 5 min and gently stirred at 30 rpm for 24 hr. Then, loaded silk fibroin nanoparticles were collected by centrifugation at 13400 rpm for 15 min. After that, the loaded silk fibroin nanoparticles were washed with water in order to remove the rest of ethanol. The determination of the loaded drug in the silk fibroin nanoparticles was determined by measuring the UV-absorbance of curcumin (421nm), indomethacin (320nm) or emodin (420nm) of the supernatant of the centrifugation (in ethanol) and the initial 1 mg/ml solution.

Drug loading content (DLC) and entrapment efficiency (EE) were calculated according to the following expressions:

$$DLC = \frac{weight\,of\,the\,drug\,in\,nanoparticles}{weight\,of\,the\,nanoparticles} \cdot 100$$

$$EE = \frac{weight\,of\,the\,drug\,in\,nanoparticles}{weight\,of\,the\,feeding\,drugs} \cdot 100$$

2.4. Release of the drug from silk fibroin nanoparticles

The release rates of curcumin, indomethacin or emodin from silk fibroin nanoparticles were then evaluated. A suspension of 20 mg of drug loaded-silk fibroin nanoparticles in 1 ml of a lightly basic solution ($2 \cdot 10^{-4}$ M NaOH) was ultra-sonicated for 1 min and then gently stirred at 30 rpm at room temperature. At a predetermined time, the suspensions were centrifuged for 15 min at 13400 rpm. The supernatant was collected to determine the concentration of drug released to the medium by UV-spectrometry. 1 ml of fresh solution was added immediately to the drug loaded-silk fibroin nanoparticles. Samples were diluted when necessary to reach an absorbance value lower than 1. Each experiment was repeated at least 6 times. The amount of drug released from the nanoparticles was expressed as a percentage of the total drug loaded into the silk fibroin nanoparticles above defined as DLC.

2.5. Molecular modeling

2.5.1. Preparation of ligands and protein

Structures of curcumin, emodin and indomethacin were fully optimized at the HF/6-31G(d) level of theory without imposing any symmetry restriction as implemented in the Gaussian09 code. Additional vibrational calculations were conducted to ascertain that each structure correspond to a minima in energy surface. Atomic charges were subsequently computed at the same level according to the Merz-Singh-Kollman ESP protocol.[39, 40] 3-D coordinates of the protein was obtained from the Protein Data Bank (PDB ID: 3UA0).[41] The protein was prepared using the Maestro program, which includes addition of the hydrogen atoms, capping of both N and C

termini of the protein and then the protonation states of all residues are defined according to neutral pH.[42]

2.5.2. Blind docking protocol

Molecular docking of curcumin, emodin and indomethacin with the silk fibroin protein and the detailed binding energy calculations were performed with Autodock Vina docking software[43] using default configuration parameters. The size of the grid box was chosen in such a way that encompasses all possible binding sites. The docking score produced by Autodock Vina was taken as the predicted value of the ligand binding energy. Only the top-ranked poses were used for structural and energy analyses. Scoring function from Vina considers Lennard-Jones term (LJ), hydrogen bonds (H-bonds), electrostatic interactions, hydrophobic stabilization, entropic penalty due to number of rotatable bonds, and internal energy of the ligand. We adopted a blind docking approach[44, 45] where multiple docking runs were started around geometric centers of all residues within the selected threshold. A histogram with the resulting distribution of binding energies and their structural clusters of poses were generated.

2.5.3. Molecular dynamics simulation

Molecular dynamics simulations were performed using the GROMACS2016 molecular dynamics package.[46-49] The topologies of the drug molecules were generated by ACPYPE[50] according to the Amber99sb[51] force field. The structure of the top pose obtained from blind docking was considered as initial protein-ligand conformation in each case. Each complex was then immersed in a triclinic box containing TIP3P[52] water molecules. Periodic boundary conditions were considered for every simulation run. Na^+ ions were added to neutralize the charge of the system. The LINCS algorithm[53] was chosen to constrain covalent bond lengths, and

an integration step of 2 fs was applied to simulate the system. Electrostatic interactions were calculated using the particle mesh Ewald (PME) method.[54] Initially, all the systems were energy minimized using steepest-descent algorithm. The minimized systems were then subjected to position restraint dynamics where the complex was restraint by employing a restraining potential. 100 ps position restrained simulation was performed in NVT ensemble using the V-rescale[55] thermostat with a coupling constant of τ = 0.5 ps. This step was followed by 900 ps equilibration in NPT ensemble. Parrinello–Rahman barostat[56] was employed with a time constant for coupling set to 2.0 ps for isotropic pressure coupling. Temperature was maintained at 300 K by employing the V-rescale thermostats with a coupling constant of τ = 0.5 ps. Final production simulations were performed with constant temperature of 300 K and constant pressure of 1 atm. using the NTP ensemble.

3. Results and discussion

3.1. Loading and release of curcumin, indomethacin and emodin by silk fibroin nanoparticle

Initially, the extinction coefficients of all the three drugs have been calculated from the absorption spectra in two different medium, listed in Table 1.

Table 1: Extinction coefficients, ε, of curcumin (λ=421nm), indomethacin (λ=320nm) and emodin (λ=420nm for ethanol and λ=520nm for $2\cdot10^{-4}$M NaOH) in ethanol and in lightly basic solution ($2\cdot10^{-4}$M NaOH).

Drug	Solvent

	Ethanol	**$2 \cdot 10^{-4}$M NaOH**
Curcumin	54.602	35.064
Indomethacin	6.164	6.277
Emodin	7.643	7.212

We have then assessed the drug loading and encapsulation efficiency of silk fibroin nanoparticles (SFNs) for all the three drugs and results are shown in Table 2. Evident from the table, SFNs appreciably load and encapsulate curcumin and indomethacin, however fails to load significant amount of emodin. Physical adsorption appears to be highly effective procedure for drug loading, at least for curcumin and indomethacin. More than 50% encapsulation efficiency has been achieved using the SFN through physical adsorption for curcumin.

Table 2: Drug Loading Content (DLC) and Encapsulation Efficiency (EE) of curcumin, indomethacin and emodin-loaded silk fibroin nanoparticles are shown. Mean values ± SD (standard deviation) are reported.

	Curcumin	**Indomethacin**	**Emodin**
DLC (%)	6.634 ± 0.133	4.001 ± 0.407	0.369 ± 0.027
EE (%)	53.750 ± 1.148	32.376 ± 3.327	2.487 ± 0.207

Drug release profiles for the three encapsulated drugs within SFNs have been investigated to elucidate the kinetic aspect of drug release. Results are shown in Fig. 1.

Prominent variations have been noted in the release profiles for three different drugs encapsulated in SFNs. Although for all the drugs within first 5 hr., burst release have been observed. After that the plateau is reached. For emodin, 100% release has been obtained in 144 hr. which probably due to the fact that SFN has the least ability to load and encapsulate this drug. Moderate observed release rate of indomethacin is in accordance with the moderate loading and encapsulation efficiency of SFNs. On the other hand, complete release of curcumin is not observed even in 168 hr., only 10% maximum release has been observed which is probably attributed to the high loading capacity and strong interactions of curcumin with silk fibroin nano-particles.

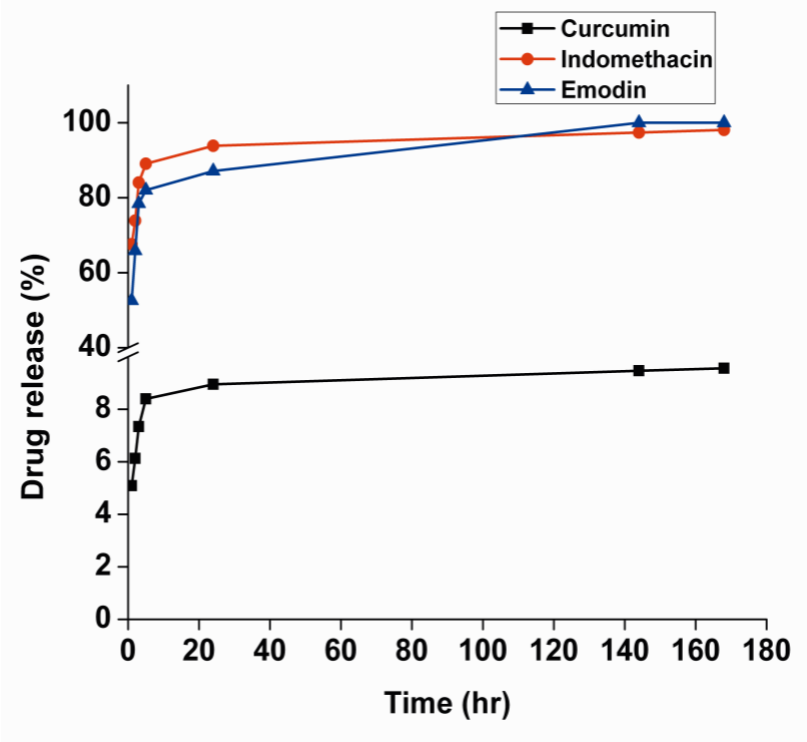

Fig. 1: Release of curcumin (in black), indomethacin (in orange) and emodin (in blue) from silk fibroin nanoparticles in lightly basic solution ($2 \cdot 10^{-4}$ M NaOH).

Clearly, the differences in the dissolution and release rate of these three amphiphilic drugs indicate that the processes are not diffusion control at least for the indomethacin and curcumin. Non-fickian diffusion implicates specific interactions with the silk-fibroin material. Therefore, we have further studied specific interactions of these drugs with the silk-fibroin using molecular docking and dynamic simulation.

3.2. Molecular docking of curcumin, indomethacin and emodin with silk-fibroin

To explore the interaction details of each drug with the silk-fibroin, molecular docking has been performed. We have adopted a blind docking procedure to explore all possible binding possibilities for each drug within the protein matrix and results are summarized in Fig. 2.

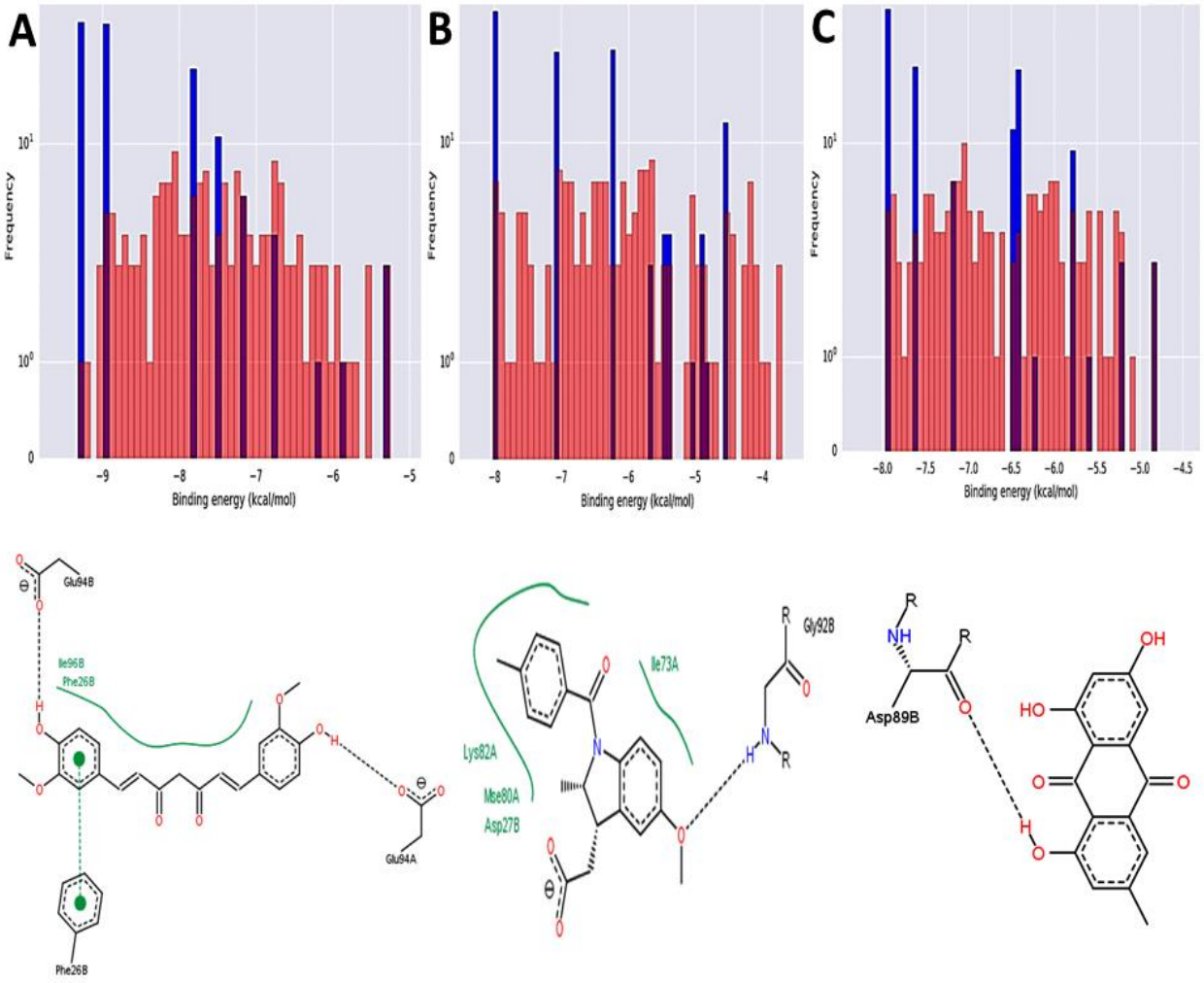

Fig. 2: Blind Docking results of selected drugs with silk fibroin protein. Upper panel represents histogram distributions of the docking score of the docked poses for (A) curcumin, (B) indomethacin and (C) emodin. Blue: clustered poses; Red: Unclustered poses. Lower panel shows the corresponding pharmacophorc feature of silk-fibroin binding obtained from the lowest energy docked pose of curcumin, indomethacin and emodin. Black dashed lines represent hydrogen bonds, green dashed lines show pi-pi interactions and green continuous lines represent hydrophobic interactions.

Evident from the figure, curcumin interacts more strongly with the protein in comparison to indomethacin and emodin. In case of curcumin, cluster analysis reveals two population clusters with the predicted interaction energy of -9.5 kcal/mol and -9 kcal/mol, respectively. Whereas the lowest predicted binding energy for indomethacin and emodin with silk-fibroin is -8 kcal/mol. The higher binding affinity of curcumin towards the silk-fibroin is attributed to higher number of hydrogen bond formation with the protein compared to emodin and indomethacin. Curcumin forms two hydrogen bonds with the protein in addition to π-π stacking interaction (Fig. 2A, lower panel). Both emodin and indomethacin form a single hydrogen bond with the protein (Fig. 2B & 2C, lower panel). However, indomethacin is involved in more number of van der Waals interactions with the receptor implicates that its binding is primarily driven by size and shape complementarity with the receptor binding site. Thus the blind docking results are fully consistent with DLC and EE values reported in Table 2.

3.3. Molecular dynamic simulation of the drug-silk fibroin complexes

Further molecular dynamic simulations have been used to assess the stability of each drug-protein complexes as well as to evaluate the primary driving force for the binding. Molecular dynamic simulations reveal that during the simulation timescale curcumin remains strongly bound to the binding site with the average center of mass distance of 0.9 Å, while translational movements have been observed for both emodin and indomethacin with the average center of mass distance of 1.8 and 2.2 Å, respectively. These facts indicate that curcumin interacts strongly with the binding site compared two other two drugs, in accordance with our blind docking results. Further we have analyzed residue fluctuations of the protein in presence of bound drugs and results are shown in Fig. 3.

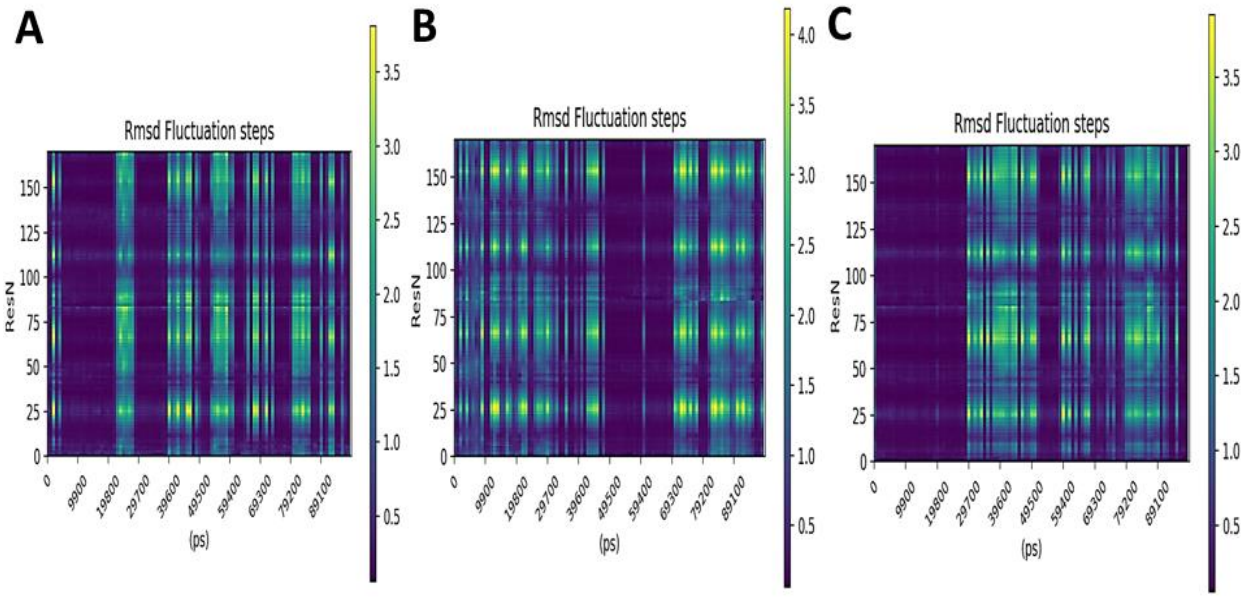

Fig. 3: Root mean square fluctuation (in Å) of each residue of the protein during the simulation time-scale when bound to curcumin (A), indomethacin (B) and emodin (C).

Evident from the figure, the protein remains stable during the simulation timescale for all the three drug-protein complexes with maximum deviations of 3.5 Å. It is to be noted that the 3-D structure of the protein is partially resolved and contains the N-terminal domain of the *Bombyx mori* fibroin heavy chains A and B. A chain contains residues 26-108 and B chain contains 23-108. Therefore the residue number in the Fig. 3 should be interpreted in terms of the appropriate residue and chain numbering of the original PDB. Among the three different fluctuation patterns, when indomethacin is bound to the active site, the protein shows highest fluctuations. Emodin induced structural deviations are least in first 30 ns of the simulation however after that the protein structure starts to deviate due to non-specific interaction of the drug to the protein matrix.

We have then evaluated the drug-protein interaction energies obtained from the MM/PBSA analysis of the simulation trajectories. Results are shown in Fig. 4.

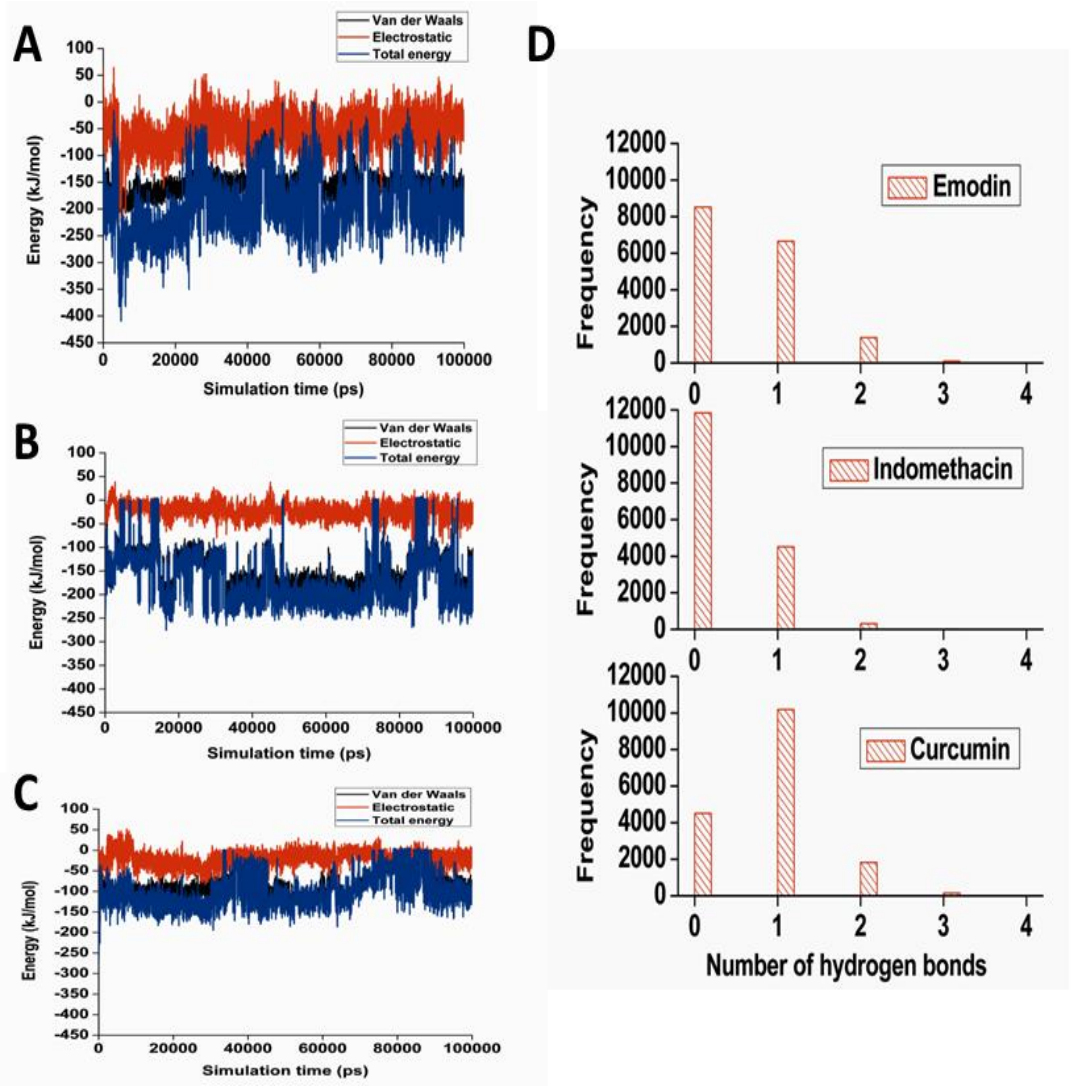

Fig. 4: Analyses of interaction energies and number of hydrogen bonds for the three drug-protein complexes using molecular dynamics simulation. Different drug-protein interaction energies obtained from the MMPBSA analysis are shown for (A) curcumin, (B) indomethacin and (C) emodin. Black curve represents van der Waals energy, while red and blue curves represent electrostatic and total energies. (D) Number of hydrogen bond distribution between each of the three drug with the protein obtained from the simulation is shown.

Clearly evident from the figure, curcumin interacts with the protein much more strongly compared to indomethacin and emodin. The total interaction energies obtained by MMPBSA analysis of the simulation trajectory for curcumin is -195 ± 56.69 kJ/mol, for indomethacin is -171 ± 53.72 kJ/mol and for emodin, it is – 100 ± 39.32 kJ/mol. Significant contribution of electrostatic interactions have been observed in case of curcumin binding with fibroin protein (Fig. 4A), compared to other two drugs which is attributed to the formation of higher number of hydrogen bonds with the protein (Fig. 2D) along with the π-π stacking interactions. Van der Waals interactions are comparable in case of both curcumin and indomethacin binding with the protein (-143.58 ± 37.39 kJ/mol for curcumin, -150.15 ± 44.40 kJ/mol for indomethacin). However, both van der Waals and electrostatic energy contributions are significantly lower in case of emodin interaction with the protein.

4. Conclusion

In this study, we have evaluated the efficacy of silk-fibroin nanoparticle as a delivery vehicle for three amphiphilic drugs, namely curcumin, indomethacin and emodin. Using a combined approach of molecular modeling, we provide the molecular level picture of the observed differential drug loading and release profiles for the three drugs within silk-fibroin matrix. Among all the three drugs, curcumin interacts strongly with the fibroin protein by forming several hydrogen bonding interactions and π-π stacking interactions. Formation of the stable complex between curcumin and silk-fibroin material justifies very slow release kinetics of the drug when encapsulated within silk-fibroin nanoparticles (SFNs). Indomethacin interacts

moderately with the SFN primarily mediated through several van der Waals interactions which accounts for its sustained release from the SFN matrix. Emodin on the other hand interacts with the fibroin protein very weakly, thus released very easily from the SFN matrix, since its release is mostly diffusion controlled.

ACKNOWLEDGEMENTS

This work was partially supported by FEDER/ERDF funds from the European Commission, the Spanish Ministry of Economy and Competitiveness (MINECO) (Ref. CTQ2014-57467-R). Mercedes G. Montalbán acknowledges support from MINECO (FPI grant, BES-2012-053267). This research was partially supported by the supercomputing infrastructure of Poznan Supercomputing Center and by the e-infrastructure program of the Research Council of Norway, and the supercomputer center of UiT - the Arctic University of Norway.

References

1. T. M. Allen and P. R. Cullis, *Science*, 2004, **303**, 1818.
2. J. Li and D. J. Mooney, *Nature Reviews Materials*, 2016, **1**, 16071.
3. J.-W. Yoo, D. J. Irvine, D. E. Discher and S. Mitragotri, *Nature Reviews Drug Discovery*, 2011, **10**, 521.

4. L. Sercombe, T. Veerati, F. Moheimani, S. Y. Wu, A. K. Sood and S. Hua, *Frontiers in Pharmacology*, 2015, **6**, 286.

5. M. Rother, M. G. Nussbaumer, K. Renggli and N. Bruns, *Chemical Society Reviews*, 2016, **45**, 6213-6249.

6. G. Leonarduzzi, G. Testa, B. Sottero, P. Gamba and G. Poli, *Current Medicinal Chemistry*, 2010, **17**, 74-95.

7. P. Mukhopadhyay, S. Maity, S. Chakraborty, R. Rudra, H. Ghodadara, M. Solanki, A. S. Chakraborti, A. K. Prajapati and P. P. Kundu, *RSC Advances*, 2016, **6**, 73210-73221.

8. V. S. S. Gonçalves, P. Gurikov, J. Poejo, A. A. Matias, S. Heinrich, C. M. M. Duarte and I. Smirnova, *European Journal of Pharmaceutics and Biopharmaceutics*, 2016, **107**, 160-170.

9. F. Ordikhani, M. Dehghani and A. Simchi, *Journal of Materials Science: Materials in Medicine*, 2015, **26**, 269.

10. C. H. Lee, H. Kim, D. V. Harburg, G. Park, Y. Ma, T. Pan, J. S. Kim, N. Y. Lee, B. H. Kim, K.-I. Jang, S.-K. Kang, Y. Huang, J. Kim, K.-M. Lee, C. Leal and J. A. Rogers, *Npg Asia Materials*, 2015, **7**, e227.

11. R. Bisht, J. K. Jaiswal, Y.-S. Chen, J. Jin and I. D. Rupenthal, *Expert Opinion on Drug Delivery*, 2016, **13**, 953-962.

12. H.-T. Chen, M. F. Neerman, A. R. Parrish and E. E. Simanek, *Journal of the American Chemical Society*, 2004, **126**, 10044-10048.

13. E. Wenk, H. P. Merkle and L. Meinel, *Journal of Controlled Release*, 2011, **150**, 128-141.

14. C. Vepari and D. L. Kaplan, *Progress in Polymer Science*, 2007, **32**, 991-1007.

15. E. M. Pritchard and D. L. Kaplan, *Expert Opinion on Drug Delivery*, 2011, **8**, 797-811.

16. B. B. Mandal and S. C. Kundu, *Biomaterials*, 2009, **30**, 2956-2965.

17. S. Hofmann, C. T. Wong Po Foo, F. Rossetti, M. Textor, G. Vunjak-Novakovic, D. L. Kaplan, H. P. Merkle and L. Meinel, *Journal of Controlled Release*, 2006, **111**, 219-227.

18. B. Kundu, R. Rajkhowa, S. C. Kundu and X. Wang, *Advanced Drug Delivery Reviews*, 2013, **65**, 457-470.

19. Y. Yang, X. Chen, F. Ding, P. Zhang, J. Liu and X. Gu, *Biomaterials*, 2007, **28**, 1643-1652.

20. L.-D. Koh, Y. Cheng, C.-P. Teng, Y.-W. Khin, X.-J. Loh, S.-Y. Tee, M. Low, E. Ye, H.-D. Yu, Y.-W. Zhang and M.-Y. Han, *Progress in Polymer Science*, 2015, **46**, 86-110.

21. V. Catto, S. Farè, I. Cattaneo, M. Figliuzzi, A. Alessandrino, G. Freddi, A. Remuzzi and M. C. Tanzi, *Materials Science and Engineering: C*, 2015, **54**, 101-111.

22. A. S. Lammel, X. Hu, S.-H. Park, D. L. Kaplan and T. R. Scheibel, *Biomaterials*, 2010, **31**, 4583-4591.

23. X. Li, Y. Liu, J. Zhang, R. You, J. Qu and M. Li, *Materials Science and Engineering: C*, 2017, **72**, 394-404.

24. T. Ak and İ. Gülçin, *Chemico-Biological Interactions*, 2008, **174**, 27-37.

25. A. Duvoix, R. Blasius, S. Delhalle, M. Schnekenburger, F. Morceau, E. Henry, M. Dicato and M. Diederich, *Cancer Letters*, 2005, **223**, 181-190.

26. K.-H. Lee, F. H. Ab. Aziz, A. Syahida, F. Abas, K. Shaari, D. A. Israf and N. H. Lajis, *European Journal of Medicinal Chemistry*, 2009, **44**, 3195-3200.

27. A. Goel, C. R. Boland and D. P. Chauhan, *Cancer Letters*, 2001, **172**, 111-118.

28. F. Yang, G. P. Lim, A. N. Begum, O. J. Ubeda, M. R. Simmons, S. S. Ambegaokar, P. P. Chen, R. Kayed, C. G. Glabe, S. A. Frautschy and G. M. Cole, *Journal of Biological Chemistry*, 2005, **280**, 5892-5901.

29. S.-Y. Park, H.-S. Kim, E.-K. Cho, B.-Y. Kwon, S. Phark, K.-W. Hwang and D. Sul, *Food and Chemical Toxicology*, 2008, **46**, 2881-2887.

30. A. Mathew, T. Fukuda, Y. Nagaoka, T. Hasumura, H. Morimoto, Y. Yoshida, T. Maekawa, K. Venugopal and D. S. Kumar, *PLOS ONE*, 2012, **7**, e32616.

31. R. K. Maheshwari, A. K. Singh, J. Gaddipati and R. C. Srimal, *Life Sciences*, 2006, **78**, 2081-2087.

32. H. Zuckerman, U. Reiss and I. Rubinstein, *Obstetrics & Gynecology*, 1974, **44**.

33. K. J. Moise, J. C. Huhta, D. S. Sharif, C.-N. Ou, B. Kirshon, N. Wasserstrum and L. Cano, *New England Journal of Medicine*, 1988, **319**, 327-331.

34. T. Pecere, M. V. Gazzola, C. Mucignat, C. Parolin, F. D. Vecchia, A. Cavaggioni, G. Basso, A. Diaspro, B. Salvato, M. Carli and G. Palù, *Cancer Research*, 2000, **60**, 2800.

35. C.-C. Lin, C.-H. Chang, J.-J. Yang, T. Namba and M. Hattori, *Journal of Ethnopharmacology*, 1996, **52**, 107-111.

36. C.-H. Chang, C.-C. Lin, J.-J. Yang, T. Namba and M. Hattori, *The American Journal of Chinese Medicine*, 1996, **24**, 139-142.

37. A. A. Lozano-Pérez, M. G. Montalbán, S. D. Aznar-Cervantes, F. Cragnolini, J. L. Cenis and G. Víllora, *Journal of Applied Polymer Science*, 2015, **132**.

38. Y.-Q. Zhang, W.-D. Shen, R.-L. Xiang, L.-J. Zhuge, W.-J. Gao and W.-B. Wang, *Journal of Nanoparticle Research*, 2007, **9**, 885-900.

39. U. C. Singh and P. A. Kollman, *Journal of Computational Chemistry*, 1984, **5**, 129-145.

40. B. H. Besler, K. M. Merz Jr and P. A. Kollman, *Journal of Computational Chemistry*, 1990, **11**, 431-439.

41. Y.-X. He, N.-N. Zhang, W.-F. Li, N. Jia, B.-Y. Chen, K. Zhou, J. Zhang, Y. Chen and C.-Z. Zhou, *Journal of Molecular Biology*, 2012, **418**, 197-207.

42. G. Madhavi Sastry, M. Adzhigirey, T. Day, R. Annabhimoju and W. Sherman, *Journal of Computer-Aided Molecular Design*, 2013, **27**, 221-234.

43. O. Trott and A. J. Olson, *Journal of Computational Chemistry*, 2010, **31**, 455-461.

44. J. Navarro-Fernández, H. Pérez-Sánchez, I. Martínez-Martínez, I. Meliciani, J. A. Guerrero, V. Vicente, J. Corral and W. Wenzel, *Journal of Medicinal Chemistry*, 2012, **55**, 6403-6412.

45. M. d. C. Martínez-Ballesta, H. Pérez-Sánchez, D. A. Moreno and M. Carvajal, *Colloids and Surfaces B: Biointerfaces*, 2016, **143**, 318-326.

46. D. Van Der Spoel, E. Lindahl, B. Hess, G. Groenhof, A. E. Mark and H. J. C. Berendsen, *Journal of Computational Chemistry*, 2005, **26**, 1701-1718.

47. S. Pronk, S. Páll, R. Schulz, P. Larsson, P. Bjelkmar, R. Apostolov, M. R. Shirts, J. C. Smith, P. M. Kasson, D. van der Spoel, B. Hess and E. Lindahl, *Bioinformatics*, 2013.

48. B. Hess, C. Kutzner, D. van der Spoel and E. Lindahl, *Journal of Chemical Theory and Computation*, 2008, **4**, 435-447.

49. H. J. C. Berendsen, D. van der Spoel and R. van Drunen, *Computer Physics Communications*, 1995, **91**, 43-56.

50. A. W. Sousa da Silva and W. F. Vranken, *BMC Research Notes*, 2012, **5**, 367.

51. S. A. Showalter and R. Brüschweiler, *Journal of Chemical Theory and Computation*, 2007, **3**, 961-975.

52. P. Mark and L. Nilsson, *The Journal of Physical Chemistry A*, 2001, **105**, 9954-9960.

53. B. Hess, H. Bekker, H. J. C. Berendsen and J. G. E. M. Fraaije, *Journal of Computational Chemistry*, 1997, **18**, 1463-1472.

54. T. Darden, D. York and L. Pedersen, *The Journal of Chemical Physics*, 1993, **98**, 10089-10092.

55. G. Bussi, D. Donadio and M. Parrinello, *The Journal of Chemical Physics*, 2007, **126**, 014101.

56. M. Parrinello and A. Rahman, *Journal of Applied Physics*, 1981, **52**, 7182-7190.